Geophys. J. R. astr. Soc. (1971) **26**, 323–339.

Acoustic-Gravity Wave Calculations in a Layer with a Linear Temperature Variation

Roy J. Greenfield and David G. Harkrider

(Received 1971 July 1)

Summary

An exact expression is obtained for the acoustic-gravity layer matrix for an atmospheric layer having a linear temperature variation. Expressions are also derived for the layer derivative matrices needed to calculate group velocity and mode excitation. The method requires the evaluation of confluent hypergeometric functions, whose series representations are rapidly convergent for layers, such as the lower thermosphere, which have large temperature gradients. The procedure allows rapid accurate calculations in studies of acoustic gravity wave propagation. The new procedure is used to calculate phase and group velocities for the GR_0 mode at periods between 5 and 12 min and gives a change in these velocities of 0·3 per cent as compared with Press and Harkrider's results.

Introduction

Over the past 10 years many theoretical and observational investigations have been made in order to improve our understanding of the generation and propagation of acoustic gravity waves in the atmosphere (Georges 1968; Pierce & Posey 1970). Many of the theoretical investigations attempted to predict the response of the atmosphere to a source such as an atmospheric explosion (Harkrider 1964; Pierce & Posey 1970; Row 1967) or to the jet stream (Claerbout 1967). Other studies were limited to the characteristics of normal modes (Press & Harkrider 1962) or to partially leaking ducts (Friedman 1966). The excitation of Rayleigh waves by atmospheric sources has also been analysed (Harkrider & Flinn 1970). The approach used in most of the above work was to apply the Thomson–Haskell method to a model of the atmosphere composed of a number of isothermal layers. This use of the isothermal layer approximation, in the limit of infinitely thin layers, has been justified by Pierce (1966). Recently Friedmond & Crawford (1968) and Vincent (1969) have numerically investigated how fine the layering must be made in order to reach a required level of accuracy. They found that for certain combinations of phase velocity and period, hundreds of layers were needed to get 0·1 per cent accuracy in the layer matrix elements.

In the solution of the period equation for normal modes or in the use of numerical integration to evaluate an internal for the pressure perturbation, such as Harkrider's (1964) equation (50), the product matrix of the individual layer matrices must be evaluated many times. Studies where many thin isothermal layers are used to model the atmosphere require large amounts of computer time. Friedman & Crawford (1968) have suggested one means of reducing the amount of computation. As an alternative approach, we show in this paper how a windless atmosphere can be

approximated with layers in which the temperature varies linearly with height. This allows a relatively small number of layers to be used, and removes the necessity to determine how thin the layering must be made to maintain accuracy. A similar approach has been used in radio propagation work and by Phinney (1970) in acoustic propagation.

Symbols

The following quantities are functions of altitude:

z vertical co-ordinate, positive upward;
w vertical particle velocity perturbation;
P_p total pressure perturbation;
χ time derivative of the dilatation;
α sound speed;
ρ atmospheric equilibrium density;
M molecular weight;
T^* real kinetic temperature in degrees kelvin.

The following are independent of altitude in a layer:

g gravity field strength, positive downward;
c phase velocity;
ω angular frequency;
γ ratio of specific heats; assumed to be 1·4;
R^* universal gas constant;
M_0 molecular weight at ground;
β downward temperature gradient;
y horizontal co-ordinate.

The following are computed quantities:

$T = [M_0/M]\, T^*$, molecular scale temperature;
$k = \omega/c$, horizontal wave number;
$\delta = g^2 k^2 - \omega^4$;

$$\beta_1 = \frac{(\gamma-1)\, g}{\gamma R^*}$$

$$m = \frac{g}{R^* \beta} - 1$$

$$Y_1 = \frac{(m+1)\, \omega^2}{\gamma g k}$$

$$Y_2 = \left(\frac{\beta_1}{\beta} - 1\right) \frac{gk}{\omega^2}$$

$$Y_3 = m+2$$

$$b = m+2$$

$$q = \tfrac{1}{2}(Y_1 + Y_2 - Y_3)$$

$$a = -q$$

$$\beta = \frac{T_1 - T_2}{z_2 - z_1}, \text{ downward temperature gradient.}$$

Layer matrix

The atmosphere is assumed to be inviscid and horizontally stratified. It is also assumed to be windless, although in a layer with constant horizontal wind velocity $\bar{v}$, the calculations below are valid with the substitution of $\omega - \mathbf{k}.\mathbf{v}$ for ω (Pierce 1966). We consider the mth layer of the atmosphere, shown in Fig. 1, in which T varies linearly with altitude. The z co-ordinate is vertically upward; the base and top of the layer are at z_1 and z_2. A new height variable is defined by

$$x = T/\beta. \tag{1}$$

In the layer the equilibrium hydrostatic density is given by (Lamb 1945, p. 545)

$$\rho(x) = \rho(x_1)\left(\frac{x_1}{x}\right)^m. \tag{2}$$

Supressing the factor $\exp[i(\omega t - ky)]$ in the solutions, the 2×2 layer matrix, a_m, for the mth layer, relates values at the top and bottom of the layer by

$$\begin{bmatrix} w_m(z_2) \\ P_p(z_2) \end{bmatrix} = a_m \begin{bmatrix} w_m(z_1) \\ P_p(z_1) \end{bmatrix}. \tag{3}$$

The w_m and P_p relate to χ by (Lamb 1945)

$$\begin{bmatrix} w_m \\ P_p \end{bmatrix} = D(z) \begin{bmatrix} \chi \\ \dot{\chi} \end{bmatrix}, \tag{4}$$

where the elements of the $D(z)$ matrix are given by

$$\left.\begin{aligned} d_{11} &= -[gk^2\alpha^2 - g\gamma\omega^2]/\delta \\ d_{12} &= \omega^2\alpha^2/\delta \\ d_{21} &= i\rho\alpha^2/\omega \\ d_{22} &= 0 \end{aligned}\right\}. \tag{5}$$

The matrix elements $(a_m)_{ij}$ are obtained by the matrizant method (e.g. Gilbert & Backus 1966). If we define

$$\psi(x) = e^{kx}\chi(x) \tag{6}$$

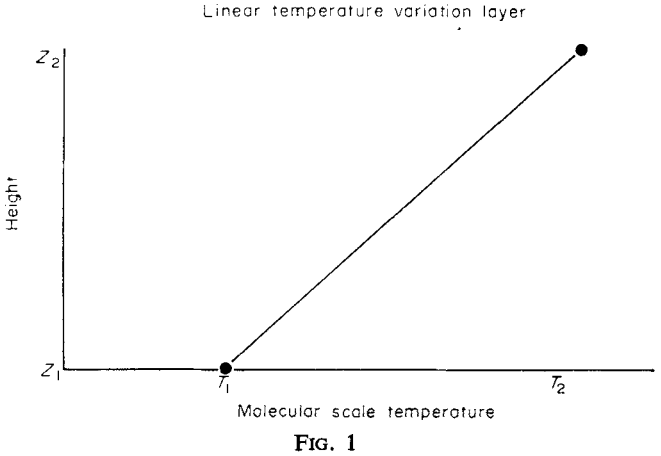

FIG. 1

then Lamb (1945) shows that $\psi(x)$ obeys

$$x\frac{\partial^2\psi}{\partial x^2}+(m+2-2kx)\frac{\partial\psi}{\partial x}+2qk\psi=0. \tag{7}$$

With the substitution $\xi\equiv 2kx$, equation (7) gives

$$\xi\frac{\partial^2\psi}{\partial\xi^2}+(m+2-\xi)\frac{\partial\psi}{\partial\xi}+q\psi=0. \tag{8}$$

The solutions to equation (8) are the confluent hypergeometric functions (Kummer's function). We take as the two linearly independent solutions for equation (8)

$$\left.\begin{aligned}\psi_1(\xi)&=M(a,b,\xi)\\ \psi_2(\xi)&=\xi^{1-b}\,e^{\xi}M(1-z,2-b,-\xi).\end{aligned}\right\} \tag{9}$$

The $\psi_1(\xi)$ and $\psi_2(\xi)$ are respectively the y_1 and y_4 solutions given by Slater (1964).

Thus, if $f_1(x)$ and $f_2(x)$ are the linearly independent solutions for $\chi(x)$ and C_1 and C_2 are constants

$$\begin{bmatrix}\chi(x)\\ \dot\chi(x)\end{bmatrix}=F(x)\begin{bmatrix}C_1\\ C_2\end{bmatrix}, \tag{10}$$

where the $F(x)$ matrix is given by

$$F(x)\equiv\begin{bmatrix}f_1(x) & f_2(x)\\ \dot f_1(x) & \dot f_2(x)\end{bmatrix}. \tag{11}$$

The expressions for the elements of the $F(x)$ matrix are

$$\left.\begin{aligned}f_{11}&=M_1\,e^{-kx}\\ f_{12}&=M_3\,e^{kx}\xi^{1-b}\\ f_{21}&=e^{-kx}\left[\frac{a}{b}2kM_2-kM_1\right]\\ f_{22}&=k\,e^{kx}\xi^{1-b}\left[\left\{1+\frac{2(1-b)}{\xi}\right\}M_3-2\left(\frac{1-a}{2-b}\right)M_4\right].\end{aligned}\right\} \tag{12}$$

The M_i are defined in Appendix A. The matrizant approach relates values at the top and bottom of the layer by

$$\begin{bmatrix}\chi(x_2)\\ \dot\chi(x_2)\end{bmatrix}=F(x_2)\,F^{-1}(x_1)\begin{bmatrix}\chi(x_1)\\ \dot\chi(x_1)\end{bmatrix}. \tag{13}$$

Combining equations (4) and (13) give

$$a_m=D_2\,F_2\,F_1^{-1}\,D_1^{-1}, \tag{14}$$

where $D_2\equiv D(x_2)$ etc.

Layer derivative matrices

Harkrider (1964) denotes the layer derivative matrices for an individual layer as $(\partial a_m/\partial k)_\omega$ and $(\partial a_m/\partial \omega)_k$. The individual elements of these derivative matrices are obtained by carrying out the indicated differentiation on the corresponding elements of the layer matrix. Harkrider (1964) then shows how the group velocity for a normal mode can be obtained by manipulation of the matrices, and how the $(\partial a_m/\partial k)_\omega$ matrices enter into the expression for the mode amplitudes. Therefore for the linear temperature variation model for the atmosphere to be useful, we require expressions for the layer derivative matrices. These are obtained by the chain rule:

$$\begin{aligned}(\partial a_m/\partial k)_\omega = {} & D_2' F_2 F_1^{-1} D_1^{-1} \\ & + D_2 F_2' F_1^{-1} D_1^{-1} \\ & + D_2 F_2 (F_1^{-1})' D_1^{-1} \\ & + D_2 F_2 F_1^{-1} (D_1^{-1})'. \end{aligned} \tag{14}$$

The prime after a matrix indicates differentiation with respect to k, with ω held constant. Writing equation (14) with the role of k and ω interchanged gives $(\partial a_m/\partial \omega)_k$.

We now give the expressions for the partial derivatives needed to evaluate $(\partial a_m/\partial k)_\omega$.

For the $D(x)$ matrix the derivatives of the elements are

$$\left.\begin{aligned} \frac{\partial d_{11}}{\partial k} &= \frac{-2gk\alpha^2}{\delta} - \frac{d_{11}}{\delta}\frac{\partial \delta}{\partial k} \\ \frac{\partial d_{12}}{\partial k} &= \frac{-d_{12}}{\delta}\frac{\partial \delta}{\partial k} \\ \frac{\partial d_{21}}{\partial k} &= \frac{\partial d_{22}}{\partial k} = 0, \end{aligned}\right\} \tag{15}$$

where

$$\frac{\partial \delta}{\partial k} = 2gk^2. \tag{16}$$

In taking the partial derivative in equations (15) and (16) and in equations (19) to (23) below, ω and x are held constant.

The partial derivatives with respect to k of the $F(x)$ matrix involve several terms. Notice that a and ξ depend on k:

$$\frac{\partial \xi}{\partial k} = 2x \tag{17}$$

$$\frac{\partial a}{\partial k} = \tfrac{1}{2}[Y_1/k - Y_2/k]. \tag{18}$$

For the f_{11} element we have

$$\frac{\partial f_{11}}{\partial k} = e^{-kx}\left[-xM_i + \frac{\partial M_i}{\partial \xi}\frac{\partial \xi}{\partial k} + \frac{\partial M_i}{\partial a}\frac{\partial a}{\partial k}\right] \tag{19}$$

$$= e^{-kx}\left[-xM_i + 2x\frac{a}{b}M_2 + P_1\frac{\partial a}{\partial k}\right]. \tag{20}$$

Equation (20) follows from equation (19) using relations given in Appendix A. The P_i are defined in the Appendices. In a similar manner the three remaining elements are

$$\frac{\partial f_{12}}{\partial k} = e^{kx}\left[\{x\xi^{1-b}+2x(1-b)\,\xi^{1-b}\}M_3+\xi^{1-b}\left\{-2x\left(\frac{1-a}{2-b}\right)M_4-P_3\frac{\partial a}{\partial k}\right\}\right] \tag{21}$$

$$\frac{\partial f_{21}}{\partial k} = e^{-kx}\left[\left\{\frac{2a}{b}-kx\frac{2a}{b}+\frac{2k}{b}\frac{\partial a}{\partial k}\right\}M_2\right.$$

$$\left.+\{-1+kx\}M_1+k\frac{2a}{b}\left\{\left(\frac{a+1}{b+1}\right)2xM_5+P_2\frac{\partial a}{\partial k}\right\}-\frac{a}{b}2xM_2-P_1\frac{\partial a}{\partial k}\right] \tag{22}$$

$$\frac{\partial f_{22}}{\partial k} = e^{kx}\left\{[\xi^{1-b}+xk\xi^{1-b}+(1-b)\,\xi^{-b}(2x)]\left[\left(1+\frac{2(1+b)}{\xi}\right)M_3-2\left(\frac{1-a}{2-b}\right)M_4\right]\right.$$

$$+(k\xi^{1-b})\left\{\frac{-2(1-b)}{\xi^2}\,2xM_3\right.$$

$$+\left[1+\frac{2(1-b)}{\xi}\right]\left[\left(\frac{1-a}{2-b}\right)M_4(-2x)+P_3\left(-\frac{\partial a}{\partial k}\right)\right]$$

$$\left.\left.-\frac{2}{(2-b)}\left(-\frac{\partial a}{\partial k}\right)M_4-2\left(\frac{1-a}{2-b}\right)\left[\left(\frac{2-a}{3-b}\right)(-2x)\,M_6+P_4\left(-\frac{\partial a}{\partial k}\right)\right]\right\}\right\}. \tag{23}$$

To evaluate equation (14) we require derivatives of $(D_1^{-1})'$ and $(F_1^{-1})'$. These are evaluated numerically with the matrix identity

$$\frac{\partial G^{-1}}{\partial s} = -[G^{-1}]\left[\frac{\partial G}{\partial s}\right][G^{-1}], \tag{24}$$

where G is any matrix and s is any scalar.

Next we give the expressions for the partial derivatives needed to evaluate $(\partial a/\partial\omega)_k$. In taking the following derivatives x and k are held constant. For the $D(x)$ matrix

$$\frac{\partial\delta}{\partial\omega} = -4\omega^3 \tag{25}$$

$$\frac{\partial d_{11}(x)}{\partial\omega} = \frac{2g\gamma\omega}{\delta}-\frac{d_{11}(x)}{\delta}\frac{\partial\delta}{\partial\omega} \tag{26}$$

$$\frac{\partial d_{12}(x)}{\partial\omega} = \frac{2\omega\alpha^2}{\delta}-\frac{d_{12}(x)}{\delta}\frac{\partial\delta}{\partial\omega} \tag{27}$$

$$\frac{\partial d_{21}(x)}{\partial\omega} = \frac{-d_{21}(x)}{\omega} \tag{28}$$

$$\frac{\partial d_{22}(x)}{\partial\omega} = 0. \tag{29}$$

The expressions for the $F(x)$ matrix are:

$$\frac{\partial f_{11}}{\partial \omega} = e^{-kx} P_1 \frac{\partial a}{\partial \omega} \tag{30}$$

where

$$\frac{\partial a}{\partial \omega} = -Y_1/\omega + Y_2/\omega \tag{31}$$

and

$$\frac{\partial f_{12}}{\partial \omega} = e^{kx} \xi^{1-b} P_3 \left(-\frac{\partial a}{\partial \omega}\right) \tag{32}$$

$$\frac{\partial f_{12}}{\partial \omega} = e^{-kx} \left[\frac{2k}{b} M_2 + \frac{2ak}{b} P_2 - kP_1\right] \left[\frac{\partial a}{\partial \omega}\right] \tag{33}$$

$$\frac{\partial f_{22}}{\partial \omega} = k e^{kx} \xi^{1-b} \left\{-\left[1 + \frac{2(1-b)}{\xi}\right] P_3 + \frac{2}{(2-b)} M_4 + 2\left(\frac{1-a}{2-b}\right) P_4\right\} \left(\frac{\partial a}{\partial \omega}\right). \tag{34}$$

Numerical tests of the accuracy of the layer matrix

The expressions given above for the layer matrix are exact; however, the evaluations of the M_i are done by a series summation, as outlined in Appendix B. For large $\xi = 2k(T/\beta)$ these series are slowly convergent. Thus roundoff and truncation errors can affect the results. To test the accuracy of the linear temperature variation layer matrix calculation we compared the resulting layer matrices to product layer matrices calculated by approximating the layer by a large number of isothermal layers, using equations (12) and (13) of Press & Harkrider (1962).

The first test was made for a linear temperature variation layer 10 km thick, with bottom and top temperatures, respectively, of 270° and 200°. The layer represents the troposphere. The layer was divided into 137 isothermal layers. For all combinations of phase velocities of 100, 150, 300 and 400 m s^{-1}, and periods of 5, 10, 20, 40 and 80 min, the two methods gave layer matrix elements which agreed to 0·01 per cent. When a period of 3·33 min and a phase velocity of 100 m s^{-1} was used the results from the two methods differed by 0·3 per cent for one of the matrix elements. This case was run again using 280 isothermal layers; these results agreed with the results for 137 isothermal layers, indicating that the isothermal results were correct and that the linear temperature variation layer method had a 0·3 per cent error.

As a second test we considered a linear temperature variation layer 60 km thick with top and bottom temperatures of 270° and 1400°, respectively. This layer fits the ARDC atmosphere (Wares *et al.* 1960) from 110 to 170 km altitude. This steep temperature gradient region is the most difficult atmospheric region to approximate with isothermal layers. Table 1 gives the difference in results for the two methods.

For a phase velocity of 100 m s^{-1} and a period of 5 min the two methods give results which differ by 3 per cent. This case was run again using 280 isothermal layers. This reduced the largest difference in any element to 1 per cent, and all the layer matrix elements could be seen to be converging to the linear temperature variation results. This indicated that the linear temperature variation results are more accurate than the isothermal layer results, and that a large number of isothermal layers must be used to get accurate results in this case.

Table 1

Largest percentage difference (for any of the four elements of the a_m matrix) between the linear temperature variation layer and isothermal layer results

Period (min)	Phase velocity (m s^{-1}) 100	150	300	400
5	3·0	0·1	0·005	0·04
10	1·5	1·0	0·015	0·01
20	0·1	0·1	0·1	0·05
40	0·05	0·15	0·1	0·01
80	0·1	0·1	0·05	0·01
80	0·1	0·1	0·05	0·01

Numerical results for atmosphere models

The multilayered dispersion program described in Press & Harkrider (1962) and Harkrider (1964) was modified to include the linear temperature variation layer algorithms along with the already present isothermal layer algorithm for zero-gradient layers. This combination of layer techniques is convenient because the linear temperature variation algorithms described in this paper are slowly convergent for small thermal gradients.

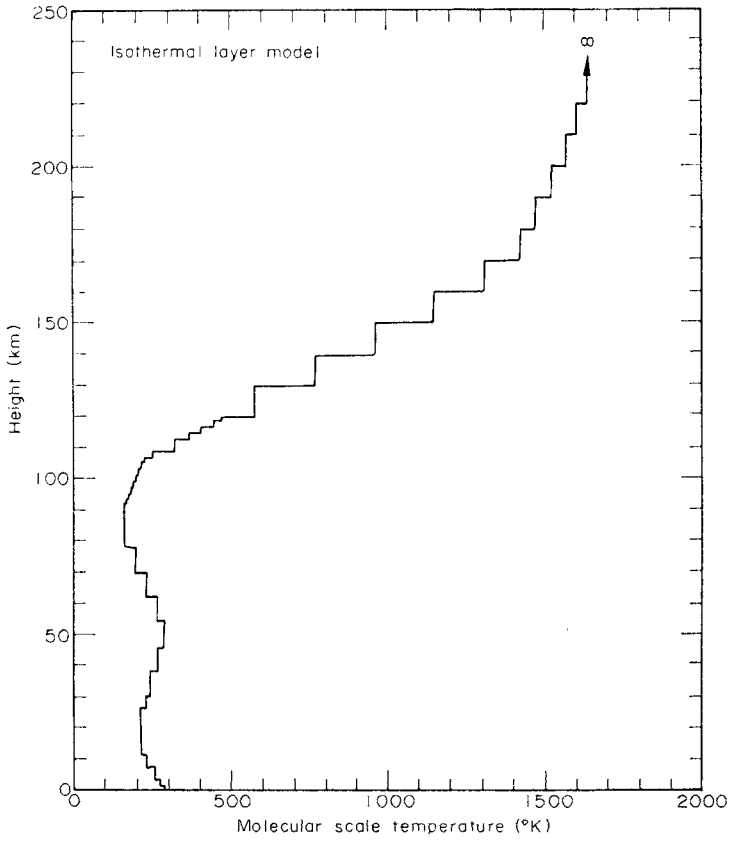

FIG. 2.

Phase velocity (c), group velocity (U), and the spectral medium response (A_A) of the GR_0 acoustic-gravity mode (Press & Harkrider 1962) were calculated for isothermal and linear temperature variation layer models of the atmosphere. For all models the atmosphere was terminated with an isothermal half-space at 220 km. Model 1 (Fig. 2) is the isothermal layered model used by Press & Harkrider (1962, their Fig. 1) and Harkrider (1964). The results for this model are given in Table 2(a). The spectral medium response, A_A, is essentially the spectral amplitude for a sea-level source and receiver, and is defined analytically by Harkrider (1964). The value of gravity, g, for each layer corresponds to that g appropriate for the layer mid-point altitude above a spherical earth.

Three basic models were used to determine the effect of neglecting non-zero temperature variations in Model 1. In Model 2 the isothermal layers from 1 to 11 km altitude were replaced by a 10 km single linear temperature variation layer. For Model 3, the entire atmosphere was replaced by linear temperature variation layers located between the dots shown in Fig. 3. In Model 4, the contiguous equal gradient layers of Model 3 were consolidated into thicker linear temperature variation layers.

The acoustic gravity modes S_0, S_1, etc. (Press & Harkrider 1962) which exist at periods less than 5 min were not calculated, since convergence in this period range required more the 100 term maximum specified in our linear temperature variation algorithms.

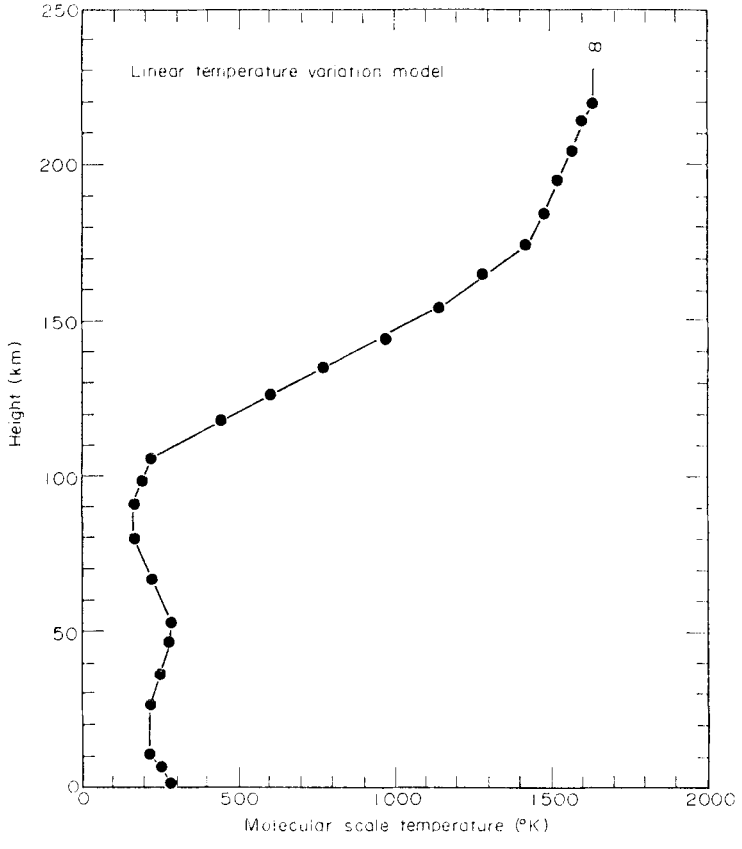

FIG. 3.

Table 2

Isothermal Model of Fig. 2

T (min)	(a) g for a spherical earth			(b) g constant		
	c (km s^{-1})	U (km s^{-1})	A_A μbar s^{-1} cm^{-2}	c (km s^{-1})	U (km s^{-1})	A_A μbar s^{-1} cm^{-2}
12·0	0·31248824	0·31219	$1{\cdot}38774\times10^{-2}$	0·31252483	0·31197	$1{\cdot}39070\times10^{-2}$
11·0	0·31246530	0·31222	$1{\cdot}38694\times10^{-2}$	0·31249392	0·31222	$1{\cdot}39237\times10^{-2}$
10·0	0·31244132	0·31218	$1{\cdot}38460\times10^{-2}$	0·31246920	0·31221	$1{\cdot}39039\times10^{-2}$
9·0	0·31241143	0·31210	$1{\cdot}38093\times10^{-2}$	0·31244002	0·31214	$1{\cdot}38684\times10^{-2}$
8·0	0·31236999	0·31197	$1{\cdot}37545\times10^{-2}$	0·31240058	0·31202	$1{\cdot}38144\times10^{-2}$
7·0	0·31230767	0·31176	$1{\cdot}36703\times10^{-2}$	0·31234202	0·31183	$1{\cdot}37315\times10^{-2}$
6·0	0·31220068	0·31132	$1{\cdot}35312\times10^{-2}$	0·31224415	0·31145	$1{\cdot}35956\times10^{-2}$
5·0	0·31193306	0·30926	$1{\cdot}32490\times10^{-2}$	0·31202452	0·31006	$1{\cdot}33332\times10^{-2}$

Table 3

Isothermal model, with linear temperature variation between 1·0 *and* 10·0 *km.*

	(a) g for a spherical earth			(b) g constant		
T (min)	c (km s^{-1})	U (km s^{-1})	A_A μbar s^{-1} cm^{-2}	c (km s^{-1})	U (km s^{-1})	A_A μbar s^{-1} cm^{-2}
12·0	0·31358167	0·31328	$1{\cdot}38378\times10^{-2}$	0·31362064	0·31313	$1{\cdot}38742\times10^{-2}$
11·0	0·31355787	0·31329	$1{\cdot}38218\times10^{-2}$	0·31359057	0·31331	$1{\cdot}38771\times10^{-2}$
10·0	0·31353185	0·31324	$1{\cdot}37900\times10^{-2}$	0·31356406	0·31328	$1{\cdot}38483\times10^{-2}$
9·0	0·31349872	0·31315	$1{\cdot}37425\times10^{-2}$	0·31353182	0·31320	$1{\cdot}38020\times10^{-2}$
8·0	0·31345272	0·31301	$1{\cdot}36732\times10^{-2}$	0·31348780	0·31307	$1{\cdot}373360\times10^{-2}$
7·0	0·31338328	0·31277	$1{\cdot}35682\times10^{-2}$	0·31342223	0·31285	$1{\cdot}36301\times10^{-2}$
6·0	0·31326459	0·31229	$1{\cdot}33979\times10^{-2}$	0·31331293	0·31243	$1{\cdot}34633\times10^{-2}$
5·0	0·31297334	0·31010	$1{\cdot}30650\times10^{-2}$	0·31307131	0·31094	$1{\cdot}31507\times10^{-2}$

Table 4

Linear temperature model, of Fig. 3

T (min)	(a) g for a spherical earth c (km s^{-1})	U (km s^{-1})	A_A μbar s^{-2} cm^{-2}	(b) g constant c (km s^{-1})	U (km s^{-1})	A_A μbar s^{-1} cm^{-2}
12·0	0·31344790	0·31314	$1·38583 \times 10^{-2}$	0·31348652	0·31300	$1·38958 \times 10^{-2}$
11·0	0·31342354	0·31315	$1·38418 \times 10^{-2}$	0·31345628	0·31317	$1·38964 \times 10^{-2}$
10·0	0·31339669	0·31310	$1·38098 \times 10^{-2}$	0·31342901	0·31314	$1·38672 \times 10^{-2}$
9·0	0·31336242	0·31301	$1·37622 \times 10^{-2}$	0·31339568	0·31305	$1·38207 \times 10^{-2}$
8·0	0·31331479	0–31286	$1·36926 \times 10^{-2}$	0·31335006	0·31291	$1·37520 \times 10^{-2}$
7·0	0·31324289	0·31261	$1·35873 \times 20^{-2}$	0·31328210	0·31269	$1·36481 \times 10^{-2}$
6·0	0·31312042	0·31210	$1·3417 \times 10^{-2}$	0·31316875	0·31226	$1·34805 \times 10^{-2}$
5·0	0·31297038	0·3106	$1·3089 \times 10^{-2}$	0·31296782	0·3108	$1·3168 \times 10^{-2}$

Table 5

Linear temperature model, large layers

(a)

g for a spherical earth*

T (min.)	*C* (km s^{-1})	*U* (km s^{-1})	A_A μbar s^{-2} cm^{-2}
12·0	0·31344799	0·31314	$1{\cdot}38570\times10^{-2}$
11·0	0·31342364	0·31315	$1{\cdot}38404\times10^{-2}$
10·0	0·31339680	0·31310	$1{\cdot}38084\times10^{-2}$
9·0	0·31336254	0·31301	$1{\cdot}37608\times10^{-2}$
8·0	0·31331492	0·31286	$1{\cdot}36912\times10^{-2}$
7·0	0·31324303	0·31261	$1{\cdot}35860\times10^{-2}$
6·0	0·31312020	0·31211	$1{\cdot}34146\times10^{-2}$
5·0	0·31298441	0·3106	$1{\cdot}309\times10^{-2}$

The inclusion of a negative temperature gradient in the lower atmosphere (Model 2) increased the plateau phase and group velocities relative to those computed from the isothermal layer Model 1 by about 0·3 per cent (Table 2(a)). For Model 3, the complete linear temperature variation model, the plateau velocities were also greater than those for Model 1 but the effect was not as large as for Model 2 (Table 4(a)). This opposing effect of about 0·03 per cent is due to the positive thermal gradients at altitude.

Strong positive gradients form anomalous regions in the atmosphere where the Brunt-Väisälä period is less than the acoustic cutoff period (Tolstoy 1967). This occurs in our models in the altitude range from 106 to 175 km. From our calculations, we see that this effect is negligible on the GR_0 mode dispersion and for near sea level sources and receivers it has a negligible effect on the GR_0 spectral amplitude, as evidenced by values of A_A in Tables 2(a), 3(a) and 4(a). The effect of placing a source or receiver in this anomalous region will be discussed in a later paper.

For Model 4, which is identical to Model 3 except for thicker temperature variation layers, the plateau velocities are slightly greater than those for Model 3 (Table 5). This is due to the difference in the gravity variation for the two models, since when *g* is constrained to be constant throughout the model, and thus the same in both models, the dispersion and spectral values for each model are identical (Table 4(b)).

In order to determine the effect of the variation of *g* with height, calculations were made for all models setting *g* constant and equal to the assumed sea-level value. The results are shown in Tables 2(b), 3(b) and 4(b). The constant-gravity models, which have a larger *g* value for each layer compared to the more realistic variation, yield slightly greater plateau velocities than their corresponding variable *g* models. This effect is less than that caused by using linear temperature variations instead of isothermal layers.

Therefore we can conclude that using more realistic linear temperature variation models increases the plateau velocities of the GR_0 acoustic gravity mode by about 0·3 per cent relative to previous isothermal larger models, and that the greatest effect is due to modelling the atmosphere with a linear thermal temperature variation in the lower 11 km. This is not surprising since the GR_0 mode is the modal equivalent of the atmospheric surface wave trapped near the Earth's surface.

Summary and conclusions

We have presented a method for computing the layer matrices and layer derivative matrices needed to calculate the phase velocity, group velocity, and mode excitation functions for acoustic gravity waves. The method is most useful in regions with large temperature gradients where the series representation of the required confluent

* Results for *g* constant are identified to those given in Table 4(b).

hypergeometric functions is rapidly convergent, and where use of the isothermal layer approximation requires very thin layering. For example, one of our calculations showed a 1·0 per cent error in the isothermal layer results when 280 layers were used to represent the E region. For this same region Friedman & Crawford (1968) determined that more than 500 layers would be needed to obtain 0·1 per cent accuracy in the layer matrix elements at a period of 58 min and a wavelength of 300 km. Friedman & Crawford presented a different method for reducing computation in comparison to the isothermal layer method. Although we are not able to assess precisely the amount of computation required for their method, it appears to be much greater than the method we present here. For small temperature gradients, at short periods or with phase velocities below $100\,\mathrm{m\,s^{-1}}$, some of the series required for the present method are poorly convergent. However, it seems likely that asymptotic methods will allow rapid evaluation of the required functions for some of the combinations of periods and phase velocities for which the series convergence is slow.

The method was presented here for a windless layer. However, we can show that in a layer with constant horizontal wind the method carries over with the substitution of $\omega - \bar{k}.\bar{V}$ for ω. At present we have not developed a method of handling a layer with changing wind shear; such a formulation would be useful in studying the effect of propagation through a critical region (Claerbout 1967).

In this work attention has been directed to real k. However, nothing in the mathematical development relies on the assumption of real k, so the method should be useful for investigations of imperfect ducting (Friedman 1966).

The expressions for the layer matrices and the layer derivative matrices were used to compute group and phase velocity curves for the GR_0 mode. The present method gave results which differed by 0·3 per cent from the results of Press & Harkrider (1962). We believe these small differences are, in the main, due to the thickness of the isothermal layers they used to represent the troposphere.

Acknowledgment

This research was partially supported by the Advanced Research Projects Agency of the Department of Defense and was monitored by the Air Force Office of Scientific Research under Contract No. F 44620–70–C–0120 with the California Institute of Technology, and under Contract F-44620-69-C-0082 with Teledyne-Geotech. Part of the computations were done at The Pennsylvania State University Computation Center.

Roy J. Greenfield:
Department of Geology and Geophysics, The Pennsylvania State University

David G. Harkrider:
Division of Geological and Planetary Sciences, California Institute of Technology

References

Claerbout, J. F., 1967. *Electromagnetic effects of atmospheric gravity waves*, Ph.D. Thesis, M.I.T., Cambridge, Mass.

Friedman, J. P., 1966. Propagation of internal gravity waves in a thermally stratified atmosphere, *J. geophys. Res.*, **71**, 1033–1054.

Friedman, J. P. & Crawford, B. W., 1968. *Acoustic-Gravity Waves in the Atmosphere*, ed. T. M. Georges, U.S. Govn. Printing Office, Washington, D.C.

Georges, T. M., 1968. *Acoustic Gravity Waves in the Atmosphere*, U.S. Govn. Printing Office, Washington, D.C.

Gilbert, F. & Backus, G. E., 1966. Propagator matrices in elastic wave theory, *Geophys.*, **31,** 326–332.
Harkrider, D. G., 1964. Theoretical and observed acoustic-gravity waves from explosive sources in the atmosphere, *J. geophys. Res.*, **69,** 5295–5321.
Harkrider, D. G. & Wells, F. J., 1968. *Acoustic-Gravity Waves in the Atmosphere*, eds. T. M. Georges, U.S. Govn. Printing Office, Washington, D.C.
Harkrider, D. G. & Flinn, E. A., 1970. Effect of crustal structure on Rayleigh waves generated by atmospheric explosions, *Rev. Geophys.*, **8,** 501–516.
Lamb, H., 1945. *Hydrodynamics*, Dover, New York, N.Y.
Phinney, R. A., 1970. Reflection of acoustic waves from a continuously varying interfacial region, *Rev. Geophys.*, **8,** 517–532.
Pierce, A. D., 1966. Justification of the use of multiple isothermal layers as an approximation to the real atmosphere for acoustic-gravity wave propagation. *Radio Sci.*, **1,** 265–267.
Pierce, A. D. & Posey, J. W., 1970. *Theoretical predictions of acoustic-gravity pressure waveforms generated by large explosions in the atmosphere*, M.I.T. Dept. of Mechanical Engr. Final Rpt., Cambridge, Mass.
Press, F. & Harkrider, D. G., 1962. Propagation of acoustic-gravity waves in the atmosphere, *J. geophys. Res.*, **67,** 3889–3908.
Row, R. V., 1967. Acoustic-gravity waves in the upper atmosphere due to a nuclear detonation and an earthquake, *J. geophys. Res.*, **72,** 1599–1610.
Slater, L. J., 1964. Confluent hypergeometric functions in *Handbook of Mathematical Functions*, U.S. Govn. Printing Office, Washington, D.C.
Tolstoy, I., 1967. Long period gravity waves in the atmosphere, *J. geophys. Res.*, **72,** 4605–4622.
Vincent, R. A., 1969. A criterion for the use of the multi-layer approximation in the study of acoustic-gravity wave propagation, *J. geophys. Res.*, **74,** 2996–3001.
Wares, G. W., Champion, K. W., Pond, H. L. & Cole, A. E., 1960. Model atmosphere, *Handbook of Geophysics*, **1–1** 1–37, The MacMillan Co., New York.

Appendix A

Definition of M_i and P_i and interrelationships

The $M(a, b, \xi)$ are Kummer's functions given by Slater (1964). This function for particular values of a, b and ξ appear repeatedly in the main body of this work, so for compactness we adopt the following notation:

$$\left.\begin{aligned}
M_1 &\equiv M(a, b, \xi) \\
M_2 &\equiv M(a+1, b+1, \xi) = \frac{b}{a}\frac{\partial M_1}{\partial \xi} \\
M_3 &\equiv M(1-a, 2-b, -\xi) \\
M_4 &\equiv M(2-a, 3-b, -\xi) = -\left(\frac{2-b}{1-a}\right)\frac{\partial M_3}{\partial \xi} \\
M_5 &\equiv M(a+2, b+2, \xi) = \left(\frac{b+1}{a+1}\right)\frac{\partial M_2}{\partial \xi} \\
M_6 &\equiv M(3-a, 4-b, -\xi) = -\left(\frac{3-b}{2-a}\right)\frac{\partial M_4}{\partial \xi}.
\end{aligned}\right\} \qquad \text{(A1)}$$

Taking partial derivatives of $M(a, b, \xi)$ with respect to a gives a new function we define as the P_i functions:

$$\left.\begin{aligned} P_1 &\equiv \frac{\partial M_1}{\partial a} \\ P_2 &\equiv \frac{\partial M_2}{\partial (a+1)} = \frac{\partial M_2}{\partial a} \\ P_3 &\equiv \frac{\partial M_3}{\partial (1-a)} = -\frac{\partial M_3}{\partial a} \\ P_4 &\equiv \frac{\partial M_4}{\partial (2-a)} = -\frac{\partial M_4}{\partial a}. \end{aligned}\right\} \tag{A2}$$

The evaluation of the M_i and P_i are considered in Appendix B.

Appendix B

Numerical evaluation of M_i and P_i

The function $M(a, b, \xi)$ is defined as (Slater 1964)

$$M(a, b, \xi) = \sum_{m=0}^{\infty} T_m, \tag{B1}$$

where

$$T_m = \frac{(a)_m \xi^m}{(b)_m m!}, \tag{B2}$$

where $$(c)_m \equiv (c)(c+1) \ldots (c+m-1) \tag{B3}$$

and $c_0 = \ldots 1$.
The series in (B1) were summed until T_L satisfied

$$|T_L| \Big/ \left| \sum_{m=0}^{L} T_M \right| < \varepsilon \tag{B4}$$

For negative ξ better numerical results were obtained by evaluating the left-hand side of the Kummer transformation (Slater 1964, p. 505)

$$e^{\xi} M(b-a, b, -\xi) = M(a, b, \xi). \tag{B5}$$

We developed the following rapid algorithm to evaluate the P_i.

$$P(a, b, \xi) = \frac{\partial M(a, b, \xi)}{\partial a}$$

$$= \sum_{m=1}^{\infty} \frac{\xi^m}{(b)_m m!} \frac{\partial (a)_m}{\partial a} \tag{B6}$$

$$\frac{\partial (a)_m}{\partial a} = (a)_m h_m \tag{B7}$$

where

$$h_m = \sum_{i=0}^{m-1} \frac{1}{a+i}$$

$$= h_{m-1} + \frac{1}{a+m-1}. \tag{B8}$$

Then

$$P(a, b, \xi) = \sum_{m=1}^{\infty} \frac{\xi^m (a)_m h_m}{(b)_m m!}. \tag{B9}$$

This series was summed and truncated by the criteria given in equation (B4). Again for negative ξ the Kummer transform was used to evaluate the P_i.

For cases when ξ is large and the series for M_i and P_i are slowly convergent, it may be practical to use one of the asymtotic expansions given by Slater (1964).